CHINESE OPTICS LETTERS

Vol. 21, No. 9 | September 2023

High-dimensional frequency conversion in a hot atomic system

Weihang Zhang (张伟航)[1,2], Yinghao Ye (叶英豪)[1,2,3], Lei Zeng (曾 雷)[1,2], Enze Li (李恩泽)[1,2], Jingyuan Peng (彭景元)[1,2], Dongsheng Ding (丁冬生)[1,2*], and Baosen Shi (史保森)[1,2**]

[1] CAS Key Laboratory of Quantum Information, University of Science and Technology of China, Hefei 230026, China

[2] CAS Center for Excellence in Quantum Information and Quantum Physics, University of Science and Technology of China, Hefei 230026, China

[3] Institute for Quantum Control and Quantum Information and School of Physics and Materials Engineering, Hefei Normal University, Hefei 230601, China

*Corresponding author: dds@ustc.edu.cn

**Corresponding author: drshi@ustc.edu.cn

Received January 6, 2023 | Accepted May 31, 2023 | Posted Online August 15, 2023

One of the major difficulties in realizing a high-dimensional frequency converter for conventional optical vortex (COV) modes stems from the difference in ring diameter of the COV modes with different topological charge numbers l. Here, we implement a high-dimensional frequency converter for perfect optical vortex (POV) modes with invariant sizes by way of the four-wave mixing (FWM) process using Bessel–Gaussian beams instead of Laguerre–Gaussian beams. The measured conversion efficiency from 1530 to 795 nm is independent of l at least in subspace $l \in \{-6, \ldots, 6\}$, and the achieved conversion fidelities for two-dimensional (2D) superposed POV states exceed 97%. We further realize the frequency conversion of 3D, 5D, and 7D superposition states with fidelities as high as 96.70%, 89.16%, and 88.68%, respectively. The proposed scheme is implemented in hot atomic vapor. It is also compatible with the cold atomic system and may find applications in high-capacity and long-distance quantum communication.

Keywords: high dimension; frequency conversion; four-wave mixing; perfect optical vortex.

DOI: 10.3788/COL202321.092701

1. Introduction

One of the most common methods for preparing conventional optical vortex (COV) modes is imprinting the helical phase pattern onto the fundamental Gaussian mode through a spatial light modulator (SLM)[1] or a spiral phase plate (SPP)[2]. Due to its unique phase structure, the COV beams have found important applications in a variety of fields, such as improved image edge detection[3] and optical tweezers for manipulating particles[4]. Because of its potential for encoding in an infinite-dimensional Hilbert space, the most extensively researched topic regarding COV modes is high-dimensional communication[5–7]. As for this topic, the implementation of high-dimensional entangled states[8], frequency conversion[9] of COV beams[10,11] with the four-wave mixing (FWM) process and quantum memory for superposed COV modes[12,13] have been realized recently.

However, the intrinsic dependence of the ring diameter of the COV modes on the topological charge number l limits its applications in scenarios where multiple modes with different values of l are simultaneously coupled into an optical system. To overcome this obstacle, various concepts of structured light fields, such as a perfect Laguerre–Gaussian beam[14,15] and a flat-top beam, have been proposed. For example, the frequency conversion of a five-dimensional (5D) superposition state has been reported using flat-top beams[16]. The most widely used kind of size-invariant light field is the perfect optical vortex (POV) beam proposed by Ostrovsky *et al.*[17]. A POV beam can be generated by Fourier transform, changing the corresponding Bessel–Gaussian (BG) beam[18,19]. It has been proved that POV beams offer advantages in establishing higher-dimensional quantum states over COV beams[20], and POV states with different values of l can also be distinguished and quantitatively identified in a projective measurement[21]. Although much pioneering research regarding the generation[19] or property analysis[22] of POV beams have been reported, in addition to its applications in optical manipulation[23,24], the high-dimensional frequency conversion of POV beams remains a meaningful topic that still needs to be studied. Here, we report a high-dimensional frequency conversion by way of the FWM process in a hot atomic system. Our solution can also be applied in a cold atomic system and thus it is useful for high-capacity and long-distance quantum communication.

As shown in Fig. 1(b), the POV beams in our experiment are generated by Fraunhofer diffracting, a BG beam embedded in

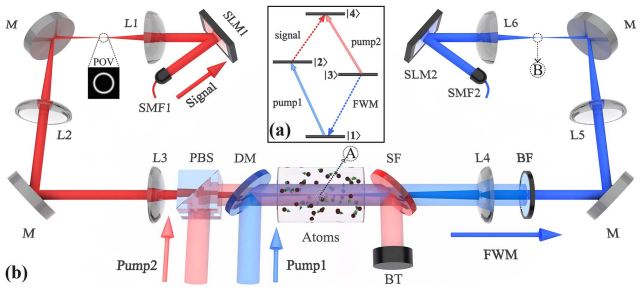

Fig. 1. (a) Energy diagram of the diamond configuration. (b) The schematic diagram of the experimental setup. SLM 1 and SLM 2, spatial light modulator; PBS, polarizing beam splitter; DM, long-pass dichroic mirror; SF, short-pass filter; BF, band-pass filter; BT, beam traps; SMF 1 and SMF 2, single-mode fiber; M, mirror. The focal lengths of lenses L1, L2, L3, L4, L5, and L6 are 75, 150, 150, 150, 150, and 75 mm, respectively.

the corresponding helical phase. The latter is prepared by passing a fundamental Gaussian beam through a SLM with hologram $\mathrm{Arg}[J_l(k_r r)e^{il\theta}]$ on it. Here, $\mathrm{Arg}[\cdots]$ represents finding the argument; J_l is lth order Bessel function of the first kind; r and θ are radial and azimuthal coordinate, respectively; and $k_r = 2.405/r_0$ is the radial wave vector with r_0 being the central core spot waist of the BG beam with $l = 0$[25]. The generated BG beam can be expressed as[26]

$$E_{\mathrm{BG}}(r,\theta) = J_l(k_r r)\exp\left(\frac{-r^2}{\omega^2}\right)\exp(il\theta), \tag{1}$$

where ω is the waist of the original fundamental Gaussian beam. The lens L1 works as a Fourier transform system to obtain he POV beam, and it can be written as[18]

$$E_{\mathrm{POV}}(r,\theta) = i^{l-1}\frac{\omega}{\omega_0}\exp(il\theta)\exp\left(\frac{-r^2+r_r^2}{\omega_0^2}\right)I_l\left(\frac{2rr_r}{\omega_0^2}\right), \tag{2}$$

where $\omega_0 = 2f/k\omega$ is the Gaussian beam waist at the rear focal plane of L1, $r_r = k_r f/k$ is the ring radius of the POV beam, $k = 2\pi/\lambda$ is the wave vector, and I_l is an lth order modified Bessel function of the first kind.

2. Experiments

The diamond-type energy configuration of the ^{85}Rb atom used in our experiment is shown in Fig. 1(a), which consists of one ground state, $|1\rangle$ ($|5S_{1/2}, F = 3\rangle$), one excited state, $|4\rangle$ ($|4D_{3/2}, F'' = 3\rangle$), and two intermediate states $|2\rangle$ ($|5P_{3/2}, F' = 3\rangle$) and $|3\rangle$ ($|5P_{1/2}, F' = 3\rangle$). The Pump 1 (780 nm), Pump 2 (1475 nm), and the signal (1530 nm) lights couple the atomic transitions of $|1\rangle \rightarrow |2\rangle$, $|3\rangle \rightarrow |4\rangle$, and $|2\rangle \rightarrow |4\rangle$ under resonance, respectively. According to the phase-matching condition of wave-vector conservation and energy conservation, a FWM light at 795 nm can be generated in the transition $|1\rangle \rightarrow |3\rangle$ through the FWM process.

The experimental setup is illustrated in Fig. 1(b). We prepare the POV beam (signal) using SLM 1 and L1 and image it into the center of a 5-cm-long ^{85}Rb vapor cell through a $4f$ system consisting of L2 and L3. The vertically polarized Pump 2 and vertically polarized Pump 1 lights are combined with the horizontally polarized signal light through a polarizing beam splitter (PBS) and a long-pass dichroic mirror (DM), respectively. The Pump 1 and Pump 2 lights propagate collinearly with the signal beam in the cell and have a waist of 1.67 mm (Pump 1) and 1.50 mm (Pump 2). The atomic cell is heated to 80°C to ensure a sufficiently high optical depth. In order to improve the signal-to-noise ratio (SNR), we use a short-pass filter and a band-pass filter to filter out the generated FWM light from the strong Pump 2 (100 mW) and Pump 1 (50 mW) lights, respectively, where Pump 1 and Pump 2 lights are the main noise sources of frequency conversion. Another $4f$ imaging system consists of L4 and L5 images and the frequency up-converted POV light (at point A) to point B for further detection with a charge-coupled device (CCD). Finally, we perform the projective measurements with a lens (L6), a SLM (SLM 2), and a single-mode fiber (SMF 2) that is placed next to the second $4f$ imaging system. The detailed projection measurement process entails passing the FWM light through SLM 2 loaded with holograms of the projected bases, which SMF 2 then collects for detection. The FWM light collected via SMF 2 is measured by a photomultiplier tube (PMT). The signal light (80 μW when it is a continuous wave) is modulated to a square-shaped pulse with a temporal width of 1 μs.

3. Results

We acquire the intensity profiles of the input (1530 nm) and converted (795 nm) POV beams through a CCD at the focal points A and B marked in Fig. 1(b), respectively. The results are shown in Fig. 2(a), and both of the ring diameters of the two beams are calculated to be around 930 μm, which indicates a spatial-mode-conserved frequency conversion. What is more, this l-independent ring diameter is consistent with the theory. Figures 2(b) and 2(c) exhibit the achieved conversion efficiency η with different l and k_r, and the main reason for the low conversion efficiency in our work is the relatively low intensity of Pump 1 and Pump 2 light, as has been discussed in Ref. [27]. The achievable power of Pump 1 and Pump 2 lights are limited by our experimental equipment. Due to the existence of the last term on right-hand side of Eq. (2), which originates from the Gaussian-shaped intensity distribution, the ring diameter will increase slowly with l, and this growth tendency becomes slower with the increase of k_r. The overlapped area between two pump beams and the POV beam changes with the increasing ring diameter, which leads to a reduced effective power of the pump light that participates in the FWM process and thus a decreased η. In comparing Figs. 2(b) and 2(c), we also find that the decreasing trend of η becomes slower as k_r increases. In this work, η barely changes when l is in the range from −6 to 6 and k_r is 24.51 mm^{-1}, as shown in Fig. 2(c).

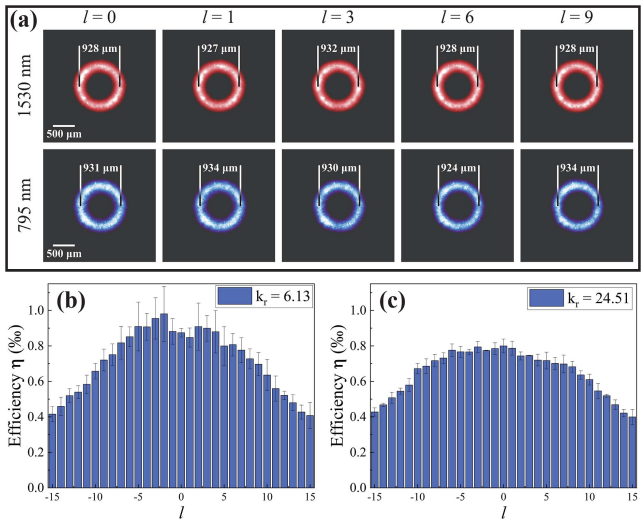

Fig. 2. (a) Intensity profiles of the input POV beams (red) and the converted POV beams (blue). (b),(c) The distribution of conversion efficiency η (unit is ‰) with different values of l in the case of $k_r = 6.13\ \mathrm{mm}^{-1}$ and $k_r = 24.51\ \mathrm{mm}^{-1}$. The η is estimated from the power and wavelength of lights before and after frequency conversion.

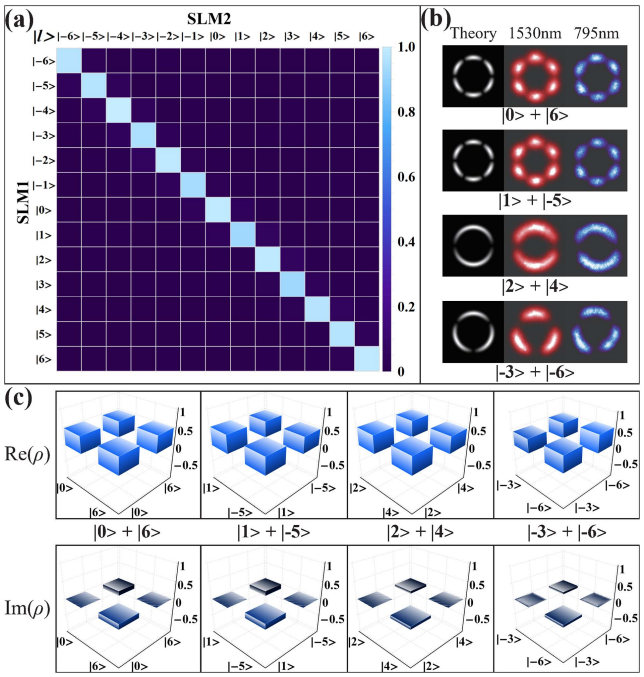

Fig. 3. (a) Cross-talk matrix between the input and the converted beams formed by the POV states in subspace $\{|-6\rangle, \ldots, |6\rangle\}$. (b) The theoretical, input, and converted beam intensity profiles of four 2D states. (c) The real and imaginary parts of the reconstructed density matrix for the four 2D states.

Figure 3(a) depicts the normalized cross-talk matrix between the input and converted POV beams, where the input and detected states $|l\rangle$ are tailored from $|-6\rangle$ to $|6\rangle$ by loading the corresponding phase hologram on SLM 1 and SLM 2, respectively. We define the SNR ($C = \sum_a M_{a,a} / \sum_{a,b} M_{a,b}$) of the cross-talk matrix to quantify the performance of our convertor. A high SNR of $C = 90.97 \pm 0.23\%$ reveals that different POV states are well distinguished from each other and have low cross-talk noise. Because of the l-independent efficiency η in the range of $l \in [-6, 6]$, we are able to realize a high-dimensional frequency conversion for a state $|\Psi\rangle$ consisting of arbitrary POV states $|l\rangle$ within this subspace. Generally speaking, a N-dimensional (ND) superposition state can be written as

$$|\Psi\rangle = \frac{1}{\sqrt{N}} \sum_{i}^{N} |l_i\rangle, \tag{3}$$

with $l_i \in [-6, 6]$.

We testify that the frequency convertor with four 2D states that have different values of $\Delta l (= |l_2| - |l_1| = 6, 4, 3, 2)$. These four states are listed as follows: $|\Psi_1\rangle = (|0\rangle + |6\rangle)/\sqrt{2}$, $|\Psi_2\rangle = (|1\rangle + |-5\rangle)/\sqrt{2}$, $|\Psi_3\rangle = (|2\rangle + |4\rangle)/\sqrt{2}$, and $|\Psi_4\rangle = (|-3\rangle + |-6\rangle)/\sqrt{2}$. Figure 3(b) shows the theoretical profile and the registered profiles of the input and converted beams of each state simultaneously. The generated beam profile is in good agreement with the theoretical simulation, and a high similarity between the intensity profiles of the input and converted beams implies a faithful conversion process. We calculate the conversion fidelity ($F = \mathrm{Tr}[\sqrt{\sqrt{\rho}\rho_0\sqrt{\rho}}]^2$) between the input and converted fields by performing a projective measurement. Here, ρ_0 and ρ are the theoretical and experimental density matrices respectively. The chosen bases for the measurement are $|l_1\rangle$, $|l_2\rangle$, $(|l_1\rangle - i|l_2\rangle)/\sqrt{2}$ and $(|l_1\rangle + |l_2\rangle)/\sqrt{2}$. The measured fidelities of $|\Psi_1\rangle$, $|\Psi_2\rangle$, $|\Psi_3\rangle$, and $|\Psi_4\rangle$ are $97.90 \pm 2.11\%$, $97.70 \pm 1.83\%$, $99.37 \pm 0.82\%$, and $99.06 \pm 0.55\%$ respectively, and the reconstructed density matrices are shown in Fig. 3(c). Our results indicate that our system has the capability to precisely convert a 2D state in the subspace $\{|-6\rangle, \ldots, |6\rangle\}$.

We then verify the validity of our system to work in 3D, 5D, and 7D states by implementing the frequency conversion process of the following states: $|3D\rangle = (|-1\rangle + |3\rangle + |-6\rangle)/\sqrt{3}$, $|5D\rangle = (|0\rangle + |1\rangle + |-3\rangle + |-5\rangle + |6\rangle)/\sqrt{5}$, and $|7D\rangle = (|0\rangle + |-1\rangle + |2\rangle + |3\rangle + |-4\rangle + |5\rangle + |-6\rangle)/\sqrt{7}$, respectively. In Fig. 4(a), the complex intensity profile of the theoretically simulated beam leads to a weak intensity part of the beam that cannot be detected by the CCD in our experiment. Thus, we observe a similarity between the theoretical and experimental beam profiles that tends to decrease as the dimensionality increases. However, the similarity between the input and converted beam profiles is still high. We chose the projected bases in the space of $\{|l_n\rangle\}, \{|l_n\rangle + \{|l_{n+1}\rangle, \ldots, |l_n\rangle + |l_N\rangle\}$, and $\{|l_n\rangle + i|l_{n+1}\rangle, \ldots, |l_n\rangle + i|l_N\rangle\}$ with $n = 1, \ldots, N$ and make projective measurements to calculate the fidelity. The reconstructed density matrix is shown in Fig. 4(b), and the fidelities are $96.7 \pm 0.83\%$, $89.16 \pm 0.32\%$, and $88.68 \pm 1.23\%$ for the 3D, 5D, and 7D states, respectively. Due to the limited fixed pixel pitch (8 μm), the distortion of the hologram displayed by the SLM becomes more obvious as the phase pattern of the superposed POV state tends to be more complex with the increased

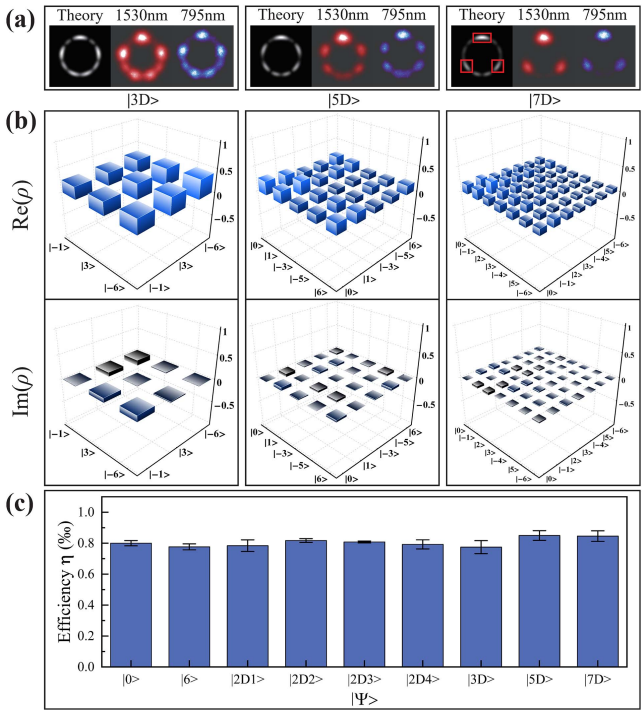

Fig. 4. (a) The theoretical, input, and converted beam intensity profiles of the 3D, 5D, and 7D states. (b) The real and imaginary parts of the reconstructed density matrix for the 3D, 5D, and 7D states. (c) The distribution of conversion efficiency η with different states $|\Psi\rangle$, where $|2D1\rangle = (|0\rangle + |6\rangle)/2$, $|2D2\rangle = (|1\rangle + |-5\rangle)/2$, $|2D3\rangle = (|2\rangle + |4\rangle)/2$, $|2D4\rangle = (|-3\rangle + |-6\rangle)/2$, $|3D\rangle = (|-1\rangle+|3\rangle + |-6\rangle)/3$, $|5D\rangle = (|0\rangle + |1\rangle + |-3\rangle + |-5\rangle + |6\rangle)/5$, and $|7D\rangle = (|0\rangle + |-1\rangle + |2\rangle + |3\rangle + |-4\rangle + |5\rangle + |-6\rangle)/7$.

number of dimensions. This results in differences in the detection efficiency of different bases during the projective measurements and causes a decrease in measured fidelity. This may be overcome using an SLM with higher pixel density or by calibrating the experimental SLM 2 before the measurement. In addition, the decrease in conversion fidelity along with the increased dimensions are also related to the minor difference in conversion efficiency for different values of l, since the ring radius of an imperfect POV field increases slightly with l[22]. By employing POV beams, we obtain a conversion fidelity over 88%, even when the number of dimension reaches 7. In comparison, the achieved fidelity decreases to 50.97% for a 3D COV state $[(|-1\rangle + |3\rangle + |-6\rangle)/\sqrt{3})]$. Note that the fidelity of the POV counterpart is 96.70%. Our system provides advantages in extending the number of dimensions of frequency conversion. Last but not least, we have obtained a nearly unchanged conversion efficiency for a superposed POV with different dimensions, as shown in Fig. 4(c).

4. Conclusion

In conclusion, we report a high-dimensional frequency conversion in a hot atomic system through the FWM process. An l-independent frequency conversion process is achieved using POV beams. We find that the range of l with constant conversion efficiency increases with the increasing k_r used in our experiment. We verify that our system has the capability to precisely convert a 2D superposition state in the subspace by performing frequency conversion on four 2D states with different values of Δl. All of the measured fidelities exceed 97%. We finally perform the frequency conversion on 3D, 5D, and 7D states and find that the conversion fidelity reaches 88.68 ± 1.23% for the 7D state. Our scheme, where the conversion efficiency is l-independent, can also be compatible with a cold atomic system and may find applications in the field of high-dimensional and long-distance quantum communication.

Acknowledgement

This work was supported by the National Key R&D Program of China (No. 2017YFA0304800), the Anhui Initiative in Quantum Information Technologies (No. AHY020200), the National Natural Science Foundation of China (Nos. U20A20218, 61722510, 11934013, 11604322, and 12204461), the Innovation Fund from CAS, Youth Innovation Promotion Association of CAS (No. 2018490), the Anhui Provincial Key Research and Development Project (No. 2022b13020002), and the Anhui Provincial Candidates for Academic and Technical Leaders Foundation (No. 2019H208).

References

1. N. Heckenberg, R. McDuff, C. P. Smith, and A. G. White, "Generation of optical phase singularities by computer-generated holograms," Opt. Lett. **17**, 221 (1992).
2. J. E. Curtis and D. G. Grier, "Structure of optical vortices," Phys. Rev. Lett. **90**, 133901 (2003).
3. S. R. Ghaleh, S. Ahmadi-Kandjani, R. Kheradmand, and B. Olyaeefar, "Improved edge detection in computational ghost imaging by introducing orbital angular momentum," Appl. Opt. **57**, 9609 (2018).
4. J. Ng, Z. Lin, and C. T. Chan, "Theory of optical trapping by an optical vortex beam," Phys. Rev. Lett. **104**, 103601 (2010).
5. I. B. Djordjevic, "Deep-space and near-Earth optical communications by coded orbital angular momentum (OAM) modulation," Opt. Express **19**, 14277 (2011).
6. A. E. Willner, H. Huang, Y. Yan, Y. Ren, N. Ahmed, G. Xie, C. Bao, L. Li, Y. Cao, Z. Zhao, J. Wang, M. P. J. Lavery, M. Tur, S. Ramachandran, A. F. Molisch, N. Ashrafi, and S. Ashrafi, "Optical communications using orbital angular momentum beams," Adv. Opt. Photon. **7**, 66 (2015).
7. C. Perumangatt, N. Lal, A. Anwar, S. G. Reddy, and R. Singh, "Quantum information with even and odd states of orbital angular momentum of light," Phys. Lett. A **381**, 1858 (2017).
8. S. Shi, M.-X. Dong, Y.-C. Yu, Y.-H. Ye, W. Zhang, K. Wang, G.-C. Guo, D.-S. Ding, and B.-S. Shi, "Entangled qutrits generated in four-wave mixing without post-selection," Opt. Express **28**, 11538 (2020).
9. D.-S. Ding, Z.-Y. Zhou, W. Huang, B.-S. Shi, X.-B. Zou, and G.-C. Guo, "Experimental up-conversion of images," Phys. Rev. A **86**, 033803 (2012).
10. D.-S. Ding, Z.-Y. Zhou, B.-S. Shi, X.-B. Zou, and G.-C. Guo, "Linear up-conversion of orbital angular momentum," Opt. Lett. **37**, 3270 (2012).
11. D.-S. Ding, Z.-Y. Zhou, B.-S. Shi, X.-B. Zou, and G.-C. Guo, "Image transfer through two sequential four-wave-mixing processes in hot atomic vapor," Phys. Rev. A **85**, 053815 (2012).
12. A. Nicolas, L. Veissier, L. Giner, E. Giacobino, D. Maxein, and J. Laurat, "A quantum memory for orbital angular momentum photonic qubits," Nat. Photonics **8**, 234 (2014).

13. Y.-H. Ye, L. Zeng, M.-X. Dong, W.-H. Zhang, E.-Z. Li, D.-C. Li, G.-C. Guo, D.-S. Ding, and B.-S. Shi, "Long-lived memory for orbital angular momentum quantum states," Phys. Rev. Lett. **129**, 193601 (2022).
14. J. Mendoza-Hernández, M. Hidalgo-Aguirre, A. I. Ladino, and D. Lopez-Mago, "Perfect Laguerre–Gauss beams," Opt. Lett. **45**, 5197 (2020).
15. X. Liu, Y. E. Monfared, R. Pan, P. Ma, Y. Cai, and C. Liang, "Experimental realization of scalar and vector perfect Laguerre–Gaussian beams," Appl. Phys. Lett. **119**, 021105 (2021).
16. S. Liu, C. Yang, Z. Xu, S. Liu, Y. Li, Y. Li, Z. Zhou, G. Guo, and B. Shi, "High-dimensional quantum frequency converter," Phys. Rev. A **101**, 012339 (2020).
17. A. S. Ostrovsky, C. Rickenstorff-Parrao, and V. Arrizón, "Generation of the "perfect" optical vortex using a liquid-crystal spatial light modulator," Opt. Lett. **38**, 534 (2013).
18. P. Vaity and L. Rusch, "Perfect vortex beam: Fourier transformation of a Bessel beam," Opt. Lett. **40**, 597 (2015).
19. N. Anaya Carvajal, C. H. Acevedo, and Y. Torres Moreno, "Generation of perfect optical vortices by using a transmission liquid crystal spatial light modulator," Int. J. Opt. **2017**, 6852019 (2017).
20. A. Anwar, S. Prabhakar, and R. Singh, "Size-invariant twisted optical modes for the efficient generation of higher-dimensional quantum states," J. Opt. Soc. Am. B **38**, 2976 (2021).
21. J. Pinnell, V. Rodríguez-Fajardo, and A. Forbes, "Quantitative orbital angular momentum measurement of perfect vortex beams," Opt. Lett. **44**, 2736 (2019).
22. J. Pinnell, V. Rodríguez-Fajardo, and A. Forbes, "How perfect are perfect vortex beams?" Opt. Lett. **44**, 5614 (2019).
23. M. Chen, M. Mazilu, Y. Arita, E. M. Wright, and K. Dholakia, "Dynamics of microparticles trapped in a perfect vortex beam," Opt. Lett. **38**, 4919 (2013).
24. G. Tkachenko, M. Chen, K. Dholakia, and M. Mazilu, "Is it possible to create a perfect fractional vortex beam?" Optica **4**, 330 (2017).
25. D. McGloin and K. Dholakia, "Bessel–Gauss beams: diffraction in a new light," Contemp. Phys. **46**, 15 (2005).
26. F. Gori, G. Guattari, and C. Padovani, "Bessel beams," Opt. Commun. **64**, 491 (1987).
27. R. Willis, F. Becerra, L. A. Orozco, and S. Rolston, "Four-wave mixing in the diamond configuration in an atomic vapor," Phys. Rev. A **79**, 033814 (2009).